

# TRUXENONE AND ISOTRUXENONE-BASED POROUS ORGANIC POLYMERS AS METAL-FREE, HETEROGENEOUS PHOTOCATALYSTS FOR VISIBLE-LIGHT-PROMOTED REDUCTION OF LUNG CANCER A549 CELLS

YongLi Tan\*, YeMu Zhu, HaiFeng Duan

*The Affiliated Changsha Central Hospital, Hengyang Medical School, University of South China, Changsha 410004, Hunan, China.*

*Corresponding author: YongLi Tan, E-mail: 37330604@qq.com*

**Abstract:** While porous materials have been widely employed in numerous fields ranging from gas adsorption and separations, light emittance, sensing to energy storage, their applications in reducing respiratory morbidity are limited. In particular, the products obtained in a controlled manner using porous materials and thus applied to limit lung cancer cells multiplication are very rare. Here we report the synthesis of two new truxenone and isotruxenone-based porous organic polymers (POPs) via Friedel-Crafts alkylation/oxidation starting from truxene and isotruxene. These networks are thermally and chemically stable, and demonstrated as the first metal-free, heterogeneous photocatalysts for visible-light-induced tunable benzylic functionalization. Moreover, both POPs can be easily recovered and reused for at least 15 times without any apparent decrease in their photocatalytic activity. The synthetic utility of this newly-developed methodology is demonstrated in the value-added functionalization of chemical feedstocks such as xylenes and mesitylene, the resulting product can be used to reduce the number of lung cancer A549 cells.

**Keywords:** A549 cells; Heterogeneous photocatalysis; Metal-Free; Porous polymers; Visible-Light

## 1 INTRODUCTION

Visible-light photocatalysis has developed into an attractive and powerful platform to promote a variety of organic transformations over the past decades.[1,2] Since most organic compounds do not absorb visible light, these synthetic manifolds largely rely on the utilization of exogenous photocatalysts to facilitate the generation of reactive intermediates. Among them, transition-metal catalysts such as ruthenium- and iridium-polypyridyl complexes are the most frequently used due to their strong absorptions, long-lived excited states, and rich photoredox properties.[3] However, the intrinsic drawbacks regarding toxicity and residue of metals impose a limit for sustainable synthesis. On the other hand, organic dyes offer a more environmental benign opportunity by harvesting solar energy for organic synthesis in a metal-free fashion.[4] Nevertheless, the corresponding reactions suffer from severe postreaction removal problems. In this regard, the development of new photocatalysts that are free of metals, recoverable and reusable with high stability, and productively form bonds is highly desirable.

To this end, porous organic polymers (POPs) that built up from organic building units have emerged as promising alternatives for photocatalysts because these materials are non-metal in nature, synthetically versatile, thermally stable and chemically robust to organic solvents, acids and bases.[5-8] More importantly, the insoluble character, permanent porosity, and tunable electrical and optical properties render them very attractive for recyclable photocatalytic heterogeneous processes.[9-21] Despite these advantages, the utilization of POPs as sustainable photocatalysts for visible-light-driven switchable organic synthesis remains previously elusive.

Given the ability in enhancing lipophilicity, metabolic stability, and receptor binding affinity, fluorine substituents are becoming increasingly prevalent in pharmaceuticals, agrochemicals, and materials.[22,23] It is thus appealing to develop efficient methodologies for the selective incorporation of fluorine into organic molecules. On the other hand, aryl ketones and aldehydes are popular structures in pharmaceuticals and biologically relevant molecules, as exemplified by commercial drugs including Bupropion, Donepezil, (S)-Ketoprofen, and Pitofenone.[24-28] Due to the abundance of C-H bonds in organic compounds, benzylic C-H functionalization constitute a practical and straightforward strategy towards these targets, thereby arousing broad interest. A variety of transition-metals as well as organic catalysts have been adopted to promote each transformation.[29-34] However, the divergent catalytic protocols that allow the synthesis of both classes of products from the same starting materials, especially with a metal-free and recyclable heterogeneous catalyst, are challenging and unknown.

Owing to the unique structures, truxene and its derivatives have found applications in a wide range of research areas, particularly in the field of organic electronics, such as organic field-effect transistors (OFETs), organic photovoltaics

(OPVs), organic light-emitting diodes (OLEDs).[35,36] Recently, they are also exploited as building blocks in the construction of porous polymers,[37-40] which serve as heterogeneous photocatalysts to promote organic transformations including oxidative coupling of benzylamine, oxidative hydroxylation of arylboronic acids, etc.[14,18,41,42] Although impressive progresses have been achieved, the known examples mainly restricted with aerobic oxidation reactions that involve the transformations of oxidative labile substrates. It is of prominent interest to discover new reactivity of (iso)truxene-based scaffolds to broaden the reaction types, particularly those allow the direct functionalization of unactivated alkyl arenes such as chemical feedstocks xylenes. Here we show modification of (iso)truxene-based porous organic polymers enables recyclable photocatalysis for metal-free and tunable benzylic functionalization of alkylarenes under visible-light irradiation. By merely changing the solvents, either benzylic fluorination or benzylic oxidation is directed, allowing the facile synthesis of fluorinated compounds and functionalized ketones or aldehydes with high efficiency. The recycling capabilities with well-retained photoactivity of both POPs over fifteen times is also illustrated. Furthermore, this method is applicable to the value-added functionalization of chemical feedstocks including xylenes and mesitylene, the resulting product can be used to reduce the number of lung cancer A549 cells.

## 2 MATERIALS AND METHODS

### 2.1 Synthesis of TRO-POP and IsoTRO-POP

FeCl<sub>3</sub> (2.13 g, 13.14 mmol, anhydrous) was added to a solution of (iso)truxene (1.5 g, 4.38 mmol) in 20 mL 1, 2-dichloroethane (DCE). After being stirred at room temperature for 15 min, dimethoxymethane (1.16 mL, 13.14 mmol) was added. Then the resulting mixture was stirred at 85 °C for 60 h (TRO-POP) or 36 h (IsoTRO-POP) to complete the cross-linking. Afterwards, the reaction mixture was cooled to room temperature and the obtained precipitate was washed with water, acetone, ethanol, ethyl acetate, dichloromethane and petroleum ether, respectively. The product was collected and dried under vacuum as brown powders (TX-POP: 1.29 g, 69% yield; IsoTX-POP: 1.38 g, 74% yield).

To a 100 mL flask were added (Iso)TX-POP (1.0 g, 2.34 mmol), CrO<sub>3</sub> (3.51 g, 35.10 mmol), and acetic acid (20 mL). The reaction mixture was refluxed for 24 h. Then, the mixture was cooled to room temperature and ethanol (15 mL) was added. After stirring for 30 min, water (15 mL) was added and the reaction mixture was stirred for additional 30 min. Further, the obtained precipitate was washed with water, acetone, ethanol, ethyl acetate, dichloromethane and petroleum ether, respectively, and then extracted in a Soxhlet extractor with acetone. The product was collected and dried under vacuum as yellow powders (TRO-POP: 0.95 g, 79% yield; IsoTRO-POP: 0.90 g, 75% yield).

### 2.2 General Procedure for Visible-Light-Induced Benzylic Fluorination

To a sealed tube were added the substrate **1** (0.2 mmol, 1.0 equiv), Selectfluor (0.24 mmol, 1.2 equiv), TRO-POP or IsoTRO-POP (5 mol%), and acetonitrile (2 mL). The reaction mixture was degassed via freeze-pump-thaw for 3 cycles. After the mixture was thoroughly degassed, the vial was sealed and positioned approximately 2~3 cm from a 12 W CFL. The mixture was stirred at room temperature for the indicated time (monitored by TLC) under nitrogen atmosphere. Afterwards, the catalyst was separated by microcentrifuge and washed with dichloromethane. Then the filtrate was concentrated by rotary evaporation and the residue was purified by silica gel flash column chromatography using methylene chloride/petroleum ether or ethyl acetate/petroleum ether as the eluent to afford the desired products **2**.

### 2.3 General Procedure for Visible-Light-Induced Benzylic Oxidation

To a sealed tube were added the substrate **1** (0.2 mmol, 1.0 equiv), Selectfluor (0.24 mmol, 1.2 equiv), TRO-POP or IsoTRO-POP (5 mol%), acetonitrile (1 mL) and H<sub>2</sub>O (1 mL). The reaction mixture was degassed via freeze-pump-thaw for 3 cycles. After the mixture was thoroughly degassed, the vial was sealed and positioned approximately 2~3 cm from a 12 W CFL. The mixture was stirred at room temperature for the indicated time (monitored by TLC) under nitrogen atmosphere. Afterwards, the catalyst was separated by microcentrifuge and washed with dichloromethane. The filtrate was diluted with H<sub>2</sub>O, and extracted with dichloromethane. Then the organic phase was concentrated by rotary evaporation and the residue was purified by silica gel flash column chromatography using methylene chloride/petroleum ether or ethyl acetate/petroleum ether as the eluent to afford the desired products **3**.

## 3 RESULTS AND DISCUSSION

### 3.1 Synthesis and Characterizations of Tro-Pop and Isotro-Pop

The synthetic routes for TRO-POP and IsoTRO-POP have been shown in Figure 1. Truxene and isotruxene were synthesized according to known procedures.[43,44] With truxene and isotruxene as the starting materials, the polymerization firstly occurs by FeCl<sub>3</sub>-promoted Friedel-Crafts alkylation with formaldehyde dimethyl acetal (FDA) as electrophile providing TX-POP and IsoTX-POP with methylene linkers. Upon treatment with super stoichiometric amount

of  $\text{CrO}_3$  and under reflux condition, TX-POP and IsoTX-POP undergo subsequent oxidation to afford truxenone and isotru xenone-based POPs as yellow and orange powders, respectively. Both POPs were insoluble in all common solvents such as *N,N*-dimethylformamide (DMF), acetonitrile, and water. Thermogravimetric analyses (TGA) showed that TRO-POP and IsoTRO-POP were stable up to 405 and 365 °C, respectively (10% weight loss, Figure 5).

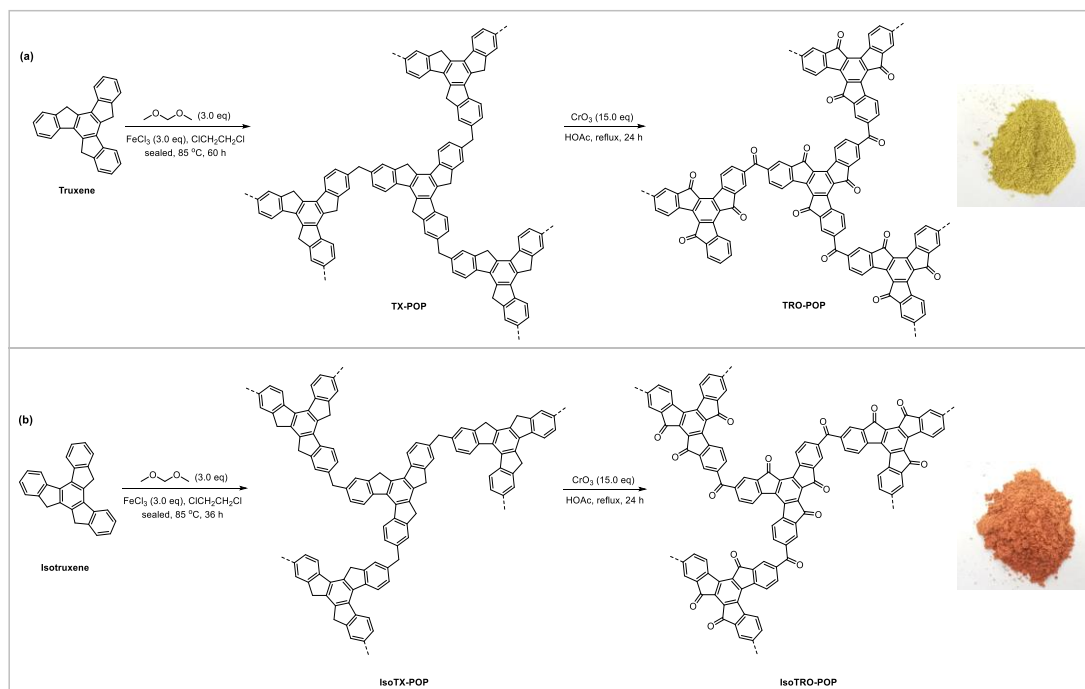


**Figure 1** Synthetic routes and idealized structures of TRO-POP and IsoTRO-POP.

The chemical structures of both POPs were elaborated by Fourier transform infrared (FTIR) analysis and  $^{13}\text{C}$  crosspolarization/magic angle spinning solid-state nuclear magnetic resonance (CP/MAS ssNMR) spectroscopy. In FTIR spectra, the peaks at  $1730\text{--}1715\text{ cm}^{-1}$  correspond to  $\text{--C=O--}$  stretching mode, supporting the existence of ketone moieties in the networks. The signals at  $1615\text{--}1610$  and  $1455\text{--}1450\text{ cm}^{-1}$  could be attributed to the vibrations of the truxenone and isotru xenone skeletons (a, Figure 2). Consistently, the CP/MAS ssNMR spectra show the signals at  $\sim 190$  ppm assigned to ketone moieties, and  $122$  to  $146$  ppm originated from the aromatic carbons of truxenone and isotru xenone (b, Figure 2). As a support, X-ray photoelectron spectroscopy (XPS) measurements disclosed that both POPs consist of carbon and oxygen elements (Figure 6). Furthermore, energy dispersive X-ray spectroscopy (EDS) and elemental analysis once again confirmed the presence of carbon and oxygen elements (Figure 8 and Table 1).

The porous feature of both POPs has been characterized by  $\text{N}_2$ -physisorption analysis (Figure 2). The  $\text{N}_2$  adsorption and desorption isotherms of both POPs indicated the presence of high percentage of micropores and minor proportion of mesopores (c and d, Figure 2). The Brunauer-Emmett-Teller (BET) specific surface areas of TRO-POP and IsoTRO-POP were measured to be  $1018$  and  $1156\text{ m}^2/\text{g}$ , with an average pore volume of  $1.43$  and  $1.44\text{ cm}^3/\text{g}$ , respectively (Figure 1). The pore diameter and distribution were determined using density functional theory (DFT) methods, revealing the majority are micropores with dimensions ranging from  $0.6$  to  $1.7\text{ nm}$  (both TRO-POP and IsoTRO-POP). Scanning electron microscopy (SEM) images demonstrated both POPs have irregular morphology (e and f, Figure 1). The amorphous structures were further confirmed by powder X-ray diffraction (PXRD) profiles, which did not exhibit any assignable peaks (Figure 10).

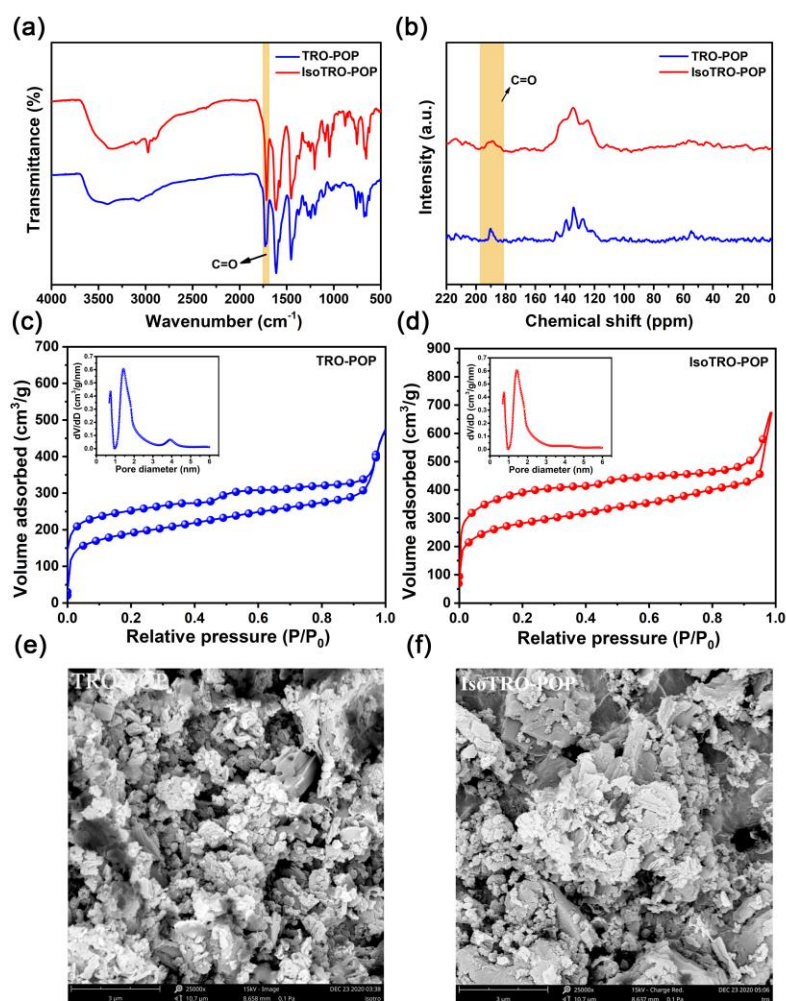


**Figure 2** (a) FTIR spectra of TRO-POP and IsoTRO-POP. (b) Solid-state  $^{13}\text{C}$  CP/MAS NMR spectra of TRO-POP and IsoTRO-POP. (c)  $\text{N}_2$ -physorption isotherms and pore size distribution curve (inset) of TRO-POP. (d)  $\text{N}_2$ -physorption isotherms and pore size distribution curve (inset) of IsoTRO-POP. (e) SEM images of TRO-POP. (f) SEM images of IsoTRO-POP.

Next, the optical and electronic properties of TRO-POP and IsoTRO-POP were probed. UV/vis diffuse reflectance spectra (DRS) of both POPs showed broad absorption bands from ultraviolet to visible light regions ( $\sim 800$  nm), which are crucial for their behavior as visible-light photocatalysts (a and b, Figure 3). It is worth noting that IsoTRO-POP exhibited an obvious redshift and enhanced absorption band compared to TRO-POP, indicating their stronger light-harvesting capability. The band gap of TRO-POP and IsoTRO-POP were calculated to be 2.36 and 2.11 eV from a Tauc plot. The conduction band minimum (CBM) of TRO-POP and IsoTRO-POP were established as -0.41 and -0.18 V via Mott-Schottky electrochemical measurements (c and d, Figure 3). On the basis of CBM and optical band gap, the valence band maximum (VBM) of TRO-POP and IsoTRO-POP were calculated to be 1.95 and 1.93 V, respectively (vs Ag/AgCl) (Figure 4).

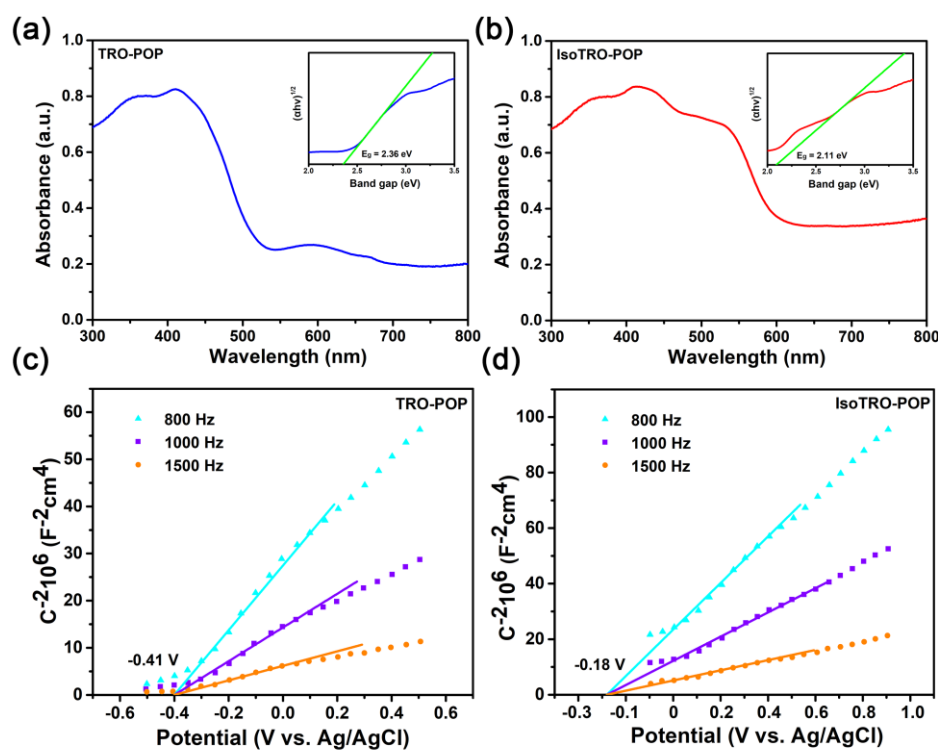


**Figure 3** (a) UV-vis diffuse reflectance spectra (DRS) and Tauc plot calculating the optical band gap (inset) of TRO-POP. (b) UV-vis diffuse reflectance spectra (DRS) and Tauc plot calculating the optical band gap (inset) of IsoTRO-POP. (c) Mott-Schottky plots of TRO-POP at frequencies 0.8, 1.0, and 1.5 kHz in a 0.2 M Na<sub>2</sub>SO<sub>4</sub> solution (pH = 7). (d) Mott-Schottky plots of IsoTRO-POP at frequencies 0.8, 1.0, and 1.5 kHz in a 0.2 M Na<sub>2</sub>SO<sub>4</sub> solution (pH = 7).

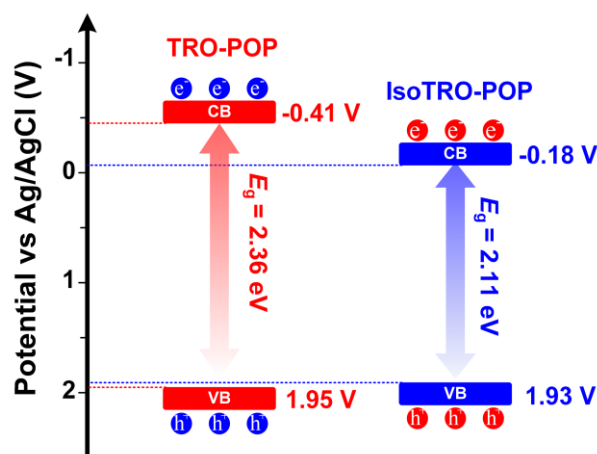


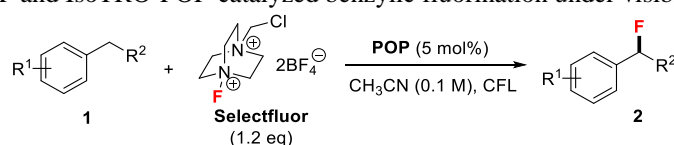
**Figure 4** Band energy diagram of TRO-POP and IsoTRO-POP.

### 3.2 Visible-Light-Promoted Benzylic Fluorination

We went on to explore the photocatalytic activity of TRO-POP and IsoTRO-POP in benzylic C-H fluorination. Gratifyingly, by using Selectfluor as the fluorine donor, benzylic fluorination of 4-ethylbiphenyl occurred smoothly in the presence of TRO-POP or IsoTRO-POP upon irradiation with a 12 W household compact fluorescent lamp (CFL), affording benzylic fluoride **2a** in 82% and 84% yield, respectively (entries 1-2, Table 1). Notably, truxene, isotruxene, TX-POP, and IsoTX-POP could not promote this reaction at all (entries 3-6, Table 1). Besides, the monomeric truxenone and isotruxenone gave poor yields under standard conditions (23-26% yield, entries 7-8, Table 1). Control experiments verified that both POPs and

visible light are essential (entries 9-11, Table 1). Then, the substrate scope was evaluated regarding both TRO-POP and IsoTRO-POP. In general, IsoTRO-POP led to better yields in a shorter reaction time compared to TRO-POP. Specifically, the ethylbenzene bearing a free carboxyl group was readily tolerated with both POPs, leading to **2b** in 78% and 82% yield, respectively (entries 12-13, Table 1). In addition to the methylene group, the methyl group could also participate in monofluorination efficiently, with good yields (88-94%) being obtained for **2c** and **2d** (entries 14-17, Table 1). The substrates possessing a variety of functionalities including a carboxylic acid, carboxylic ester, ketone, or tertiary alcohol underwent benzylic fluorination smoothly, affording the corresponding fluorinated products **2e-2h** in good yields (78-90%, entries 18-25, Table 1). Notably, the catalyst loading of both POPs could be further decreased to 0.5 mol% and 0.1 mol%, respectively, in which comparable results were achieved with a relatively prolonged reaction time (Figure 5).

**Table 1** TRO-POP and IsoTRO-POP-catalyzed benzylic fluorination under visible-light irradiation<sup>a</sup>



entry	substrates ( <b>1</b> )	products ( <b>2</b> )	catalyst	yield <sup>b</sup>
1			TRO-POP	82% (3.5 h)
2			IsoTRO-POP	84% (1.2 h)
3			Truxene	0
4			Isotruxene	0
5			TX-POP	0
6			IsoTX-POP	0
7			Truxenone	23% (1.2 h)
8			Isotruxenone	26% (1.2 h)
9 <sup>c</sup>			/	0
10 <sup>d</sup>			TRO-POP	0
11 <sup>d</sup>			IsoTRO-POP	0
12			TRO-POP	78% (21.2 h)
13			IsoTRO-POP	82% (16.2 h)
14			TRO-POP	92% (5.5 h)
15			IsoTRO-POP	94% (3.2 h)
16			TRO-POP	88% (4.3 h)
17			IsoTRO-POP	90% (2.2 h)
18			TRO-POP	82% (67.3 h)
19			IsoTRO-POP	88% (64 h)
20			TRO-POP	78% (69.3 h)
21			IsoTRO-POP	79% (65 h)
22			TRO-POP	83% (20.2 h)
23			IsoTRO-POP	86% (16 h)
24			TRO-POP	84% (22.5 h)
25			IsoTRO-POP	90% (15.3 h)

<sup>a</sup>General conditions: **1** (0.2 mmol), **Selectfluor** (0.24 mmol) in CH<sub>3</sub>CN (2.0 mL, 0.1 M) were stirred at room temperature under the irradiation with a 12 W CFL. <sup>b</sup>Isolated yield. <sup>c</sup>In the absence of TRO-POP or IsoTRO-POP. <sup>d</sup>In dark.

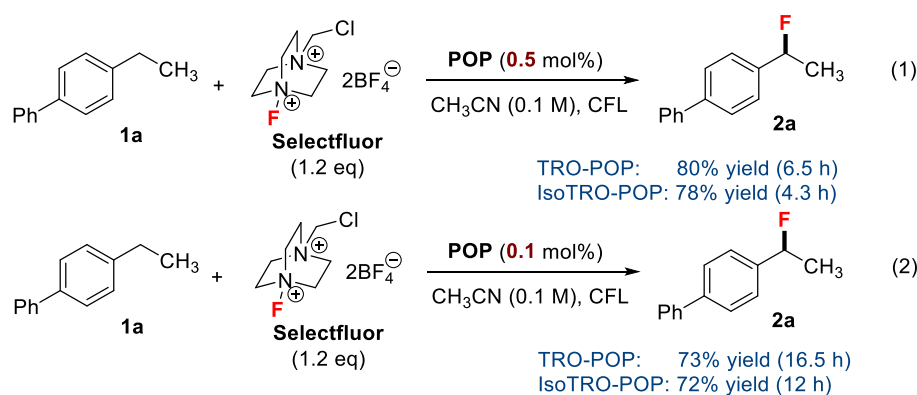
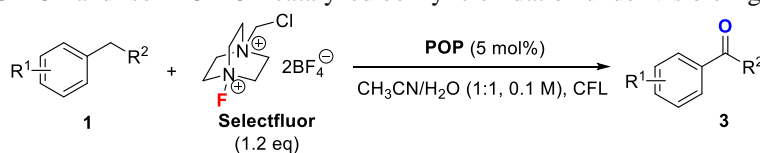


**Figure 5** Investigation of decreased catalyst loading for benzylic fluorination.

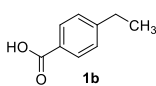
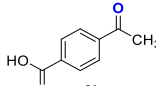
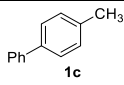
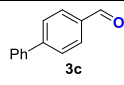
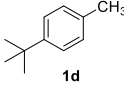
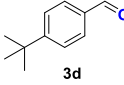
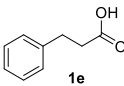
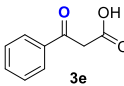
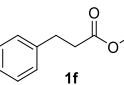
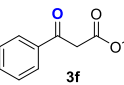
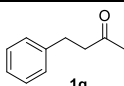
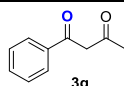
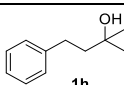
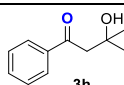
### 3.3 Visible-Light-Promoted Benzylic Oxidation

Interestingly, the fluorination products were completely switched to oxidation products when the solvent was changed to the mixture of acetonitrile and water. This result encouraged us to explore the generality of visible-light-promoted benzylic oxidation as two sets of completely different compounds can be obtained from the same starting materials under superficially similar conditions but in a controllable fashion. With TRO-POP and IsoTRO-POP as the catalysts and the mixture of acetonitrile and water as the solvent, 4-ethylbiphenyl proceeded effectively to afford the expected aryl ketone **3a** in 79% yield and 81% yield, respectively (entries 1-2, Table 2). Similarly, truxene, isotruxene, TX-POP, IsoTX-POP, truxenone, and isotruxenone proved less effective in promoting benzylic oxidations compared to that of TRO-POP and IsoTRO-POP (0-21% yields, entries 3-8, Table 2). Control experiments indicated that light and photocatalysts were indispensable for the formation of the benzylic oxidation product (entries 9-11, Table 2). Besides, the arene could be easily modified with electron-withdrawing and -donating groups (-COOH, -<sup>t</sup>Bu) (entries 12-17, Table 2). Methylbenzenes **1c** and **1d** are also good substrates, delivering the corresponding aldehydes **3c** and **3d** in 80-90% yields under the catalysis of each POP. Gratifyingly, the compounds bearing a variety of functionalities such as carboxylic acid (**1e**), carboxylic ester (**1f**), ketone (**1g**), or tertiary alcohol (**1h**) were well tolerated (entries 18-25, Table 2). The resultant 1,3-dicarbonyl compounds and  $\beta$ -hydroxyketones, which are common building blocks in organic synthesis could be constructed in a concise manner by directly editing C-H bond. When lowering the catalyst loading of both POPs to 0.5 mol% and 0.1 mol% respectively, the benzylic oxidation reactions proceeded smoothly to give the desired aryl ketone **3a** in good yields albeit with an extended reaction time (Scheme 3).

**Table 2** TRO-POP and IsoTRO-POP-catalyzed benzylic oxidation under visible-light irradiation<sup>a</sup>



entry	substrates ( <b>1</b> )	products ( <b>2</b> )	catalyst	yield <sup>b</sup>
1			TRO-POP	79% (15 h)
2			IsoTRO-POP	81% (12 h)
3			Truxene	0 (24 h)
4			Isotruxene	0 (24 h)
5			TX-POP	0 (24 h)
6			IsoTX-POP	0 (24 h)
7			Truxenone	19% (12 h)
8			Isotruxenone	21% (12 h)
9 <sup>c</sup>			/	0 (24 h)
10 <sup>d</sup>			TRO-POP	0 (24 h)
11 <sup>d</sup>			IsoTRO-POP	0 (24 h)

12			TRO-POP	75% (24 h)
13			IsoTRO-POP	79% (20 h)
14			TRO-POP	86% (10 h)
15			IsoTRO-POP	90% (8 h)
16			TRO-POP	80% (9 h)
17			IsoTRO-POP	85% (5 h)
18			TRO-POP	76% (76 h)
19			IsoTRO-POP	83% (70 h)
20			TRO-POP	70% (72 h)
21			IsoTRO-POP	76% (67 h)
22			TRO-POP	80% (26 h)
23			IsoTRO-POP	85% (19 h)
24			TRO-POP	79% (27 h)
25			IsoTRO-POP	86% (18 h)

<sup>a</sup>General conditions: **1** (0.2 mmol), **Selectfluor** (0.24 mmol) in CH<sub>3</sub>CN/H<sub>2</sub>O (1:1, 0.1 M) were stirred at room temperature under the irradiation with a 12 W CFL. <sup>b</sup>Isolated yield. <sup>c</sup>In the absence of TRO-POP or IsoTRO-POP. <sup>d</sup>In dark.

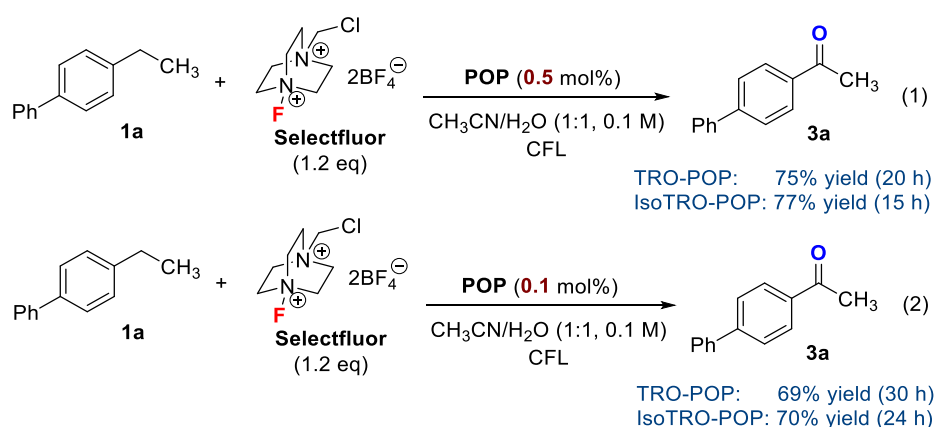
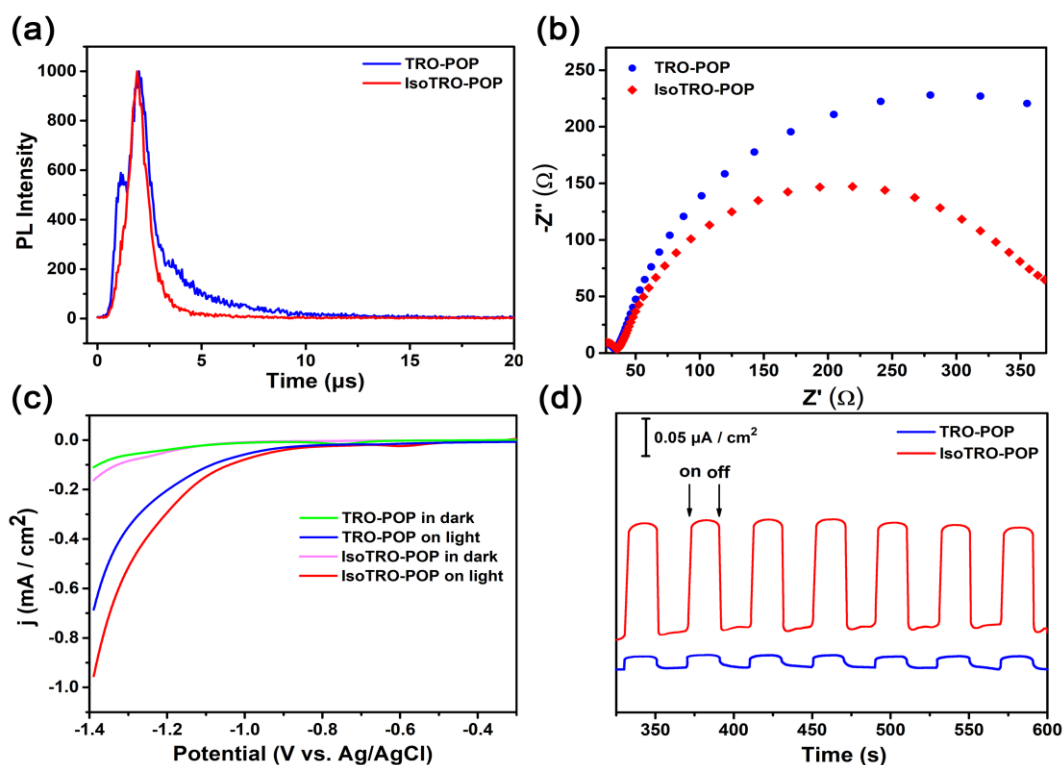


**Figure 6** Investigation of decreased catalyst loading for benzylic oxidation.

### 3.4 Mechanistic Investigation

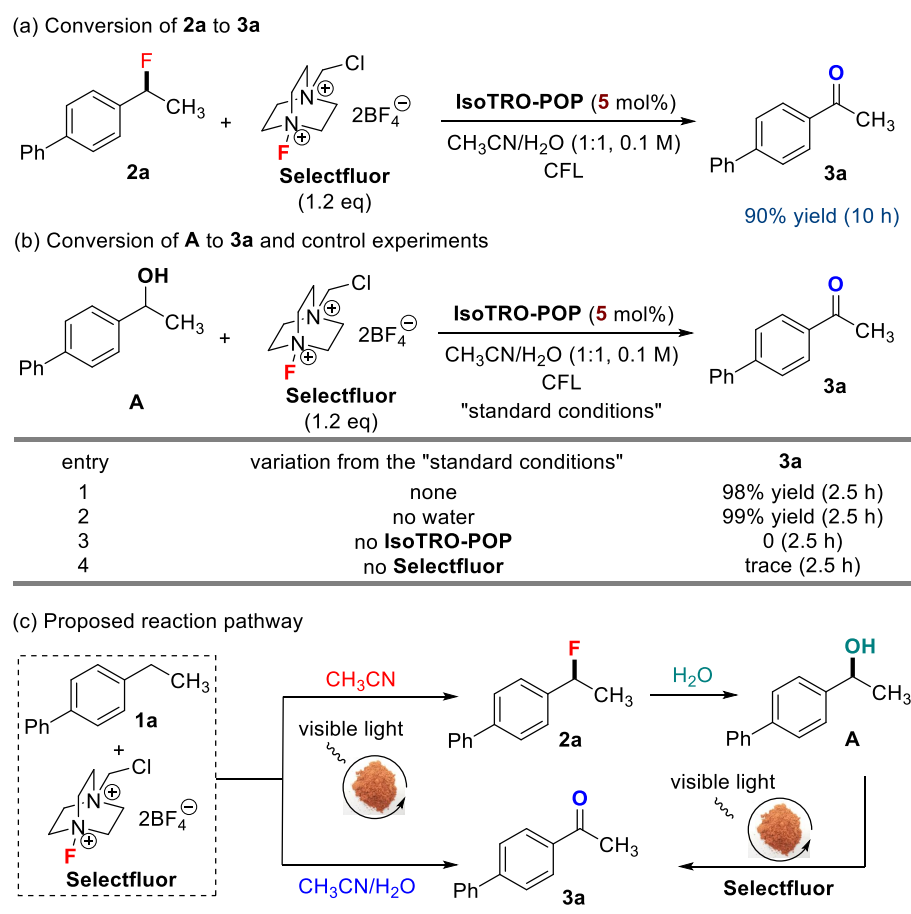
After examining the scope with respect to both benzylic fluorination and benzylic oxidation reactions, it was discovered IsoTRO-POP gave superior results in comparison with TRO-POP. To gain insights into the photocatalytic activity of both materials, the separation efficiency of photogenerated electron-hole pairs was evaluated (Figure 7). The time-resolved fluorescence spectra (TRPL) disclosed the average TRPL lifetime of IsoTRO-POP ( $\tau = 0.613 \mu\text{s}$ ) was shorter than that of TRO-POP ( $\tau = 2.017 \mu\text{s}$ ), implying that IsoTRO-POP had a more prominent non-radiative rate (a, Figure 7). The electrochemical impedance spectroscopy (EIS) indicated IsoTRO-POP had a smaller radius of a semicircular Nyquist plot compared to that of TRO-POP, which manifested a lower resistance in charge transfer for IsoTRO-POP (b, Figure 7). The linear sweep voltammetry (LSV) curves of TRO-POP and IsoTRO-POP showed the photocurrents under light irradiation were much higher than that in the dark, and meanwhile the current of IsoTRO-POP was higher than that of TRO-POP regardless of light illumination (c, Figure 7). These results suggested a better photo-electric activity of IsoTRO-POP. Consistently, IsoTRO-POP displayed a significantly enhanced photocurrent response compared to TRO-POP as shown in

Figure 7 d. Based on these studies, IsoTRO-POP bearing oligofluorene skeletons is believed to be more favored in photo-induced charge generation, transfer and separation, which can be explained for its better performance in photocatalysis.



**Figure 7** (a) Time-resolved PL spectra for TRO-POP and IsoTRO-POP. (b) EIS Nyquist plots of TRO-POP and IsoTRO-POP. (c) LSV curves of TRO-POP and IsoTRO-POP under visible-light irradiation and in the dark. (d) Photocurrent tests.

The second concern arises from the phenomenon that the product distribution can be diverted completely by simply changing the solvents. To probe the process, the reaction between **1a** and **Selectfluor** employing IsoTRO-POP as the catalyst and the mixture of acetonitrile and water as the solvent was monitored. It was observed that fluorination product **2a** was formed at the very beginning and gradually disappeared. Meanwhile, 1-([1,1'-biphenyl]-4-yl)ethan-1-ol (**A**) was detected. These insights suggested that **1a** might undergo nucleophilic substitution in the presence of water and serve as an intermediate in a sequential approach to benzylic oxidation. Accordingly, both **2a** and **A** were subjected to the standard conditions. As expected, the oxidation product **3a** was obtained in each case (Figure 8 a and entry 1 of Figure 8 b). Notably, the control experiments verified both IsoTRO-POP and **Selectfluor** were required for the subsequent oxidation (entries 2-4, Figure 8 b). Based on these observations, a plausible reaction pathway for the divergent synthesis was proposed, as depicted in Figure 8 c. By using acetonitrile as the solvent, TRO-POP and IsoTRO-POP-catalyzed benzylic fluorination occurs to afford fluorination product **2a** exclusively. When water is added as the co-solvent, a sequence including benzylic fluorination/nucleophilic substitution with water/oxidation takes place instead.



**Figure 8** Preliminary mechanistic studies. (a) Conversion of **2a** to **3a**. (b) Conversion of **A** to **3a** and control experiments. (c) Proposed reaction pathway.

### 3.5 Recyclability Tests

Next, the recycling experiments for the divergent reactions were performed by using centrifugation to recover the catalysts. It was found that both TRO-POP and IsoTRO-POP could promote the benzylic fluorination and oxidation for at least 15 recycling times without a significant drop in the yields (Figure 9 and Tables 2). And there is no apparent change in the FTIR spectra or UV/vis DRS of the spent TRO-POP and IsoTRO-POP after 15 cycles. As such, both POPs serve as highly efficient, robust, stable, recyclable, and low-cost pure organic heterogeneous photocatalysts for visible-light-induced tunable benzylic functionalization.

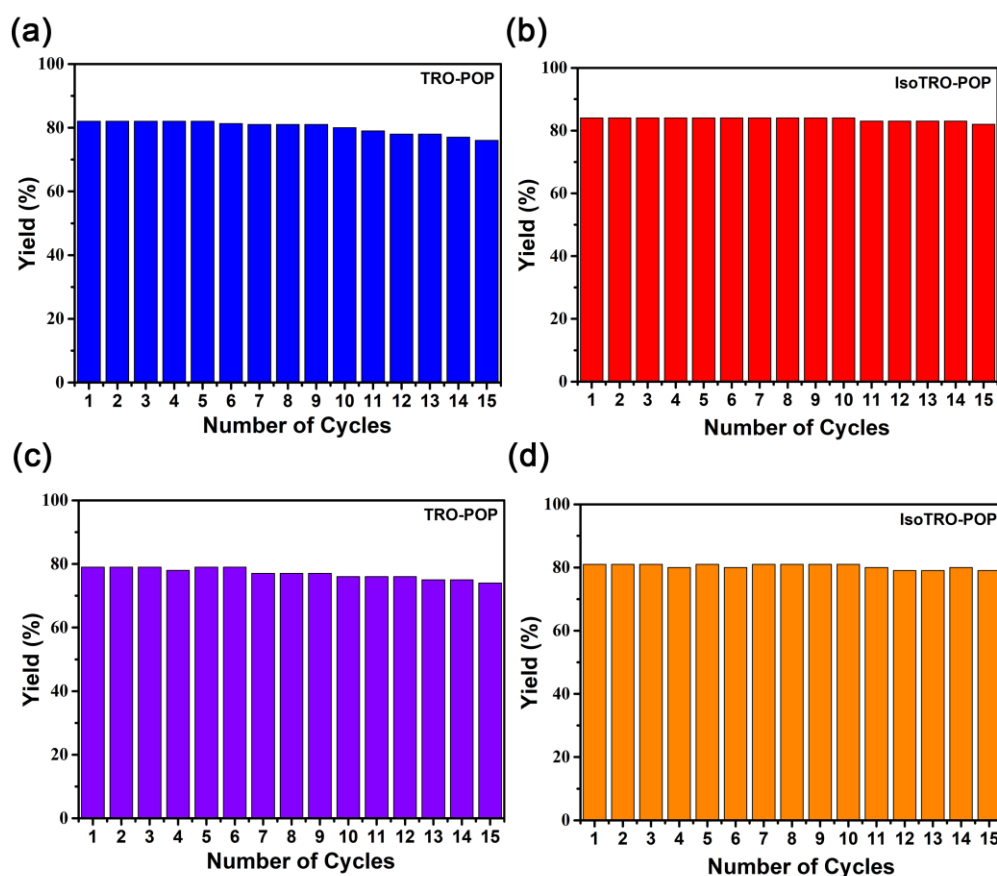


**Figure 9** (a) and (b) Recyclability tests of TRO-POP and IsoTRO-POP in the benzylic fluorination reaction. Reaction conditions: 1a (0.2 mmol), Selectfluor (0.24 mmol) in CH<sub>3</sub>CN (2.0 mL, 0.1 M) were stirred at room temperature under the irradiation with a 12 W CFL. (c) and (d) Recyclability tests of TRO-POP and IsoTRO-POP in the benzylic oxidation reaction. Reaction conditions: 1a (0.2 mmol), Selectfluor (0.24 mmol) in CH<sub>3</sub>CN/H<sub>2</sub>O (1:1, 0.1 M) were stirred at room temperature under the irradiation with a 12 W CFL.

### 3.6 Synthetic Utility

To demonstrate the amenability of this divergent strategy for value-added functionalization of chemical feedstocks, we subjected *o*-xylene, *m*-xylene, *p*-xylene, and mesitylene to standard conditions (Figure 10 a and Figure 10 b). In all cases, the fluorine and ketone moieties were introduced selectively using different solvents, leading to the corresponding multi-fluorinated derivatives and polyaldehydes in good yields, respectively. Notably, both types of products are of importance in the areas of pharmaceuticals, agrochemicals, and materials science. Moreover, 1,3,5-tri(4-methylphenyl)benzene (**6**) was tested under conditions for benzylic oxidation. To our delight, the expected product 1,3,5-Tris(4-formylphenyl)benzene (**7**), which is a versatile synthon for the preparation of COFs can be obtained in good yield (Figure 10 c).

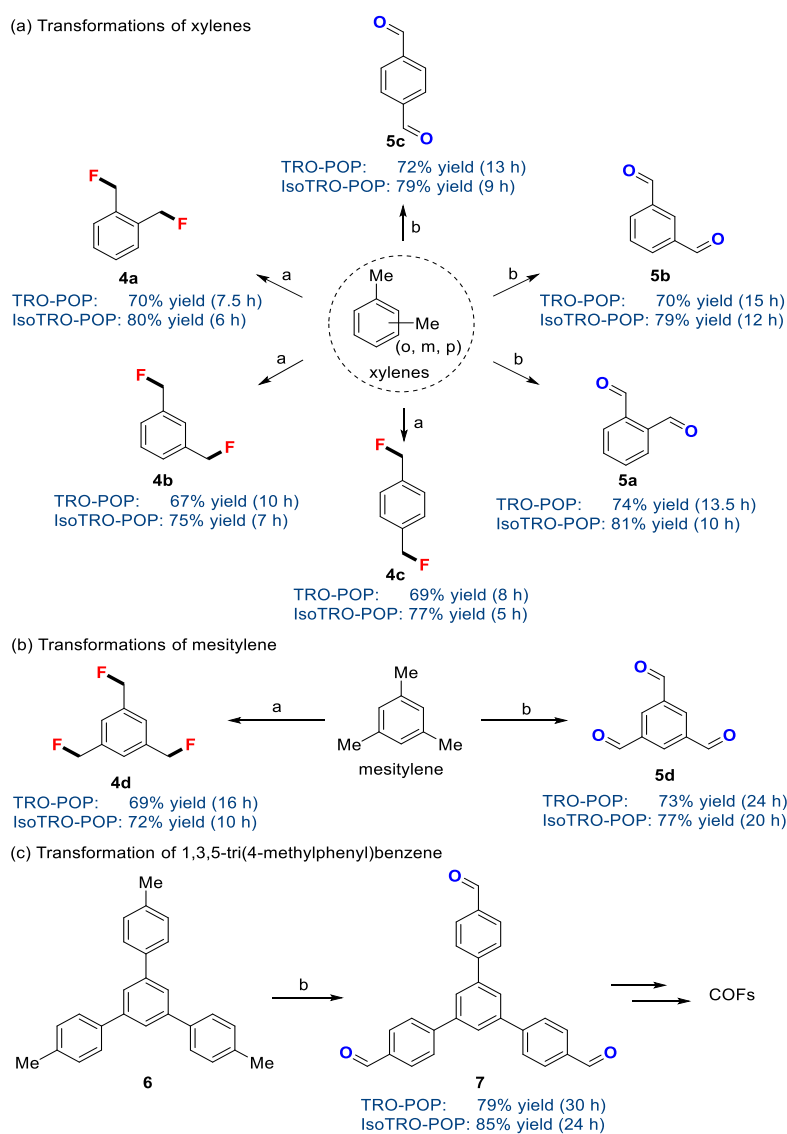


**Figure 10** Transformations. Condition a: **1** (0.2 mmol), Selectfluor (0.48 or 0.72 mmol) in CH<sub>3</sub>CN (0.1 M) were stirred at room temperature under the irradiation with a 12 W CFL. Condition b: **1** (0.2 mmol), Selectfluor (0.48 or 0.72 mmol) in CH<sub>3</sub>CN/H<sub>2</sub>O (1:1, 0.1 M) were stirred at room temperature under the irradiation with a 12 W CFL.

## 4 CONCLUSIONS

In conclusion, we have introduced a simple method for the synthesis of two new truxenone and isotruxenone-based POPs (TRO-POP and IsoTRO-POP) with truxene and isotruxene as the starting materials. These POPs are utilized as the first metal-free, heterogeneous photocatalysts for visible-light-induced tunable benzylic functionalization. By switching the solvents, either benzylic fluorination or benzylic oxidation is directed, resulting in the divergent synthesis of two types of products, namely fluorinated compounds and functionalized ketones or aldehydes in good to excellent yields from the same set of substrates. Decrease of the catalyst loading and recycling experiments reveal both POPs display excellent stability, high efficiency, and robust reusability. In addition, the optical and electronic characterizations suggest IsoTRO-POP is more in favor of charge transfer and separation, giving rise to superior photocatalytic activity compared to that of TRO-POP. Preliminary mechanistic studies account for the divergent reaction pathway. When water is used as the co-solvent, a sequence involving benzylic fluorination/nucleophilic substitution with water/oxidation occurs instead. Finally, the synthetic utility is illustrated in the elaborations of chemical feedstocks such as xylenes and mesitylene, and the product was used to reduce the reproduction of lung cancer A549 cells. A variety of important multi-fluorinated compounds as well as

polyaldehydes can be accessed in a precisely controlled fashion with a single operation. To the best of our knowledge, this is the first example that porous materials can catalyze tunable organic synthesis under visible-light irradiation. Our lab is focusing on reducing the incidence of respiratory disease with porous organic polymers.

## COMPETING INTERESTS

The authors have no relevant financial or non-financial interests to disclose.

## ACKNOWLEDGEMENT

Thank you for the laboratory provided by the Institute of Geriatrics, Hunan Provincial People's Hospital.

## REFERENCES

- [1] T.P. Yoon, M.A. Ischay, J. Du. Visible Light Photocatalysis as a Greener Approach to Photochemical Synthesis. *Nat. Chem.* 2010, 2(7): 527-532. DOI: <https://doi.org/10.1038/nchem.687>.
- [2] J. Xuan, W.J. Xiao. Visible-Light Photoredox Catalysis. *Angew. Chem. Int. Ed.* 2012, 51(28): 6828-6838. DOI: <https://doi.org/10.1002/anie.201200223>.
- [3] C.K. Prier, D.A. Rankic, D.W.C. MacMillan. Visible Light Photoredox Catalysis with Transition Metal Complexes: Applications in Organic Synthesis. *Chem. Rev.* 2013, 113(7): 5322-5363. DOI: <https://doi.org/10.1021/cr300503r>.
- [4] N.A. Romero, D.A. Nicewicz. Organic Photoredox Catalysis. *Chem Rev.* 2016, 116(17): 10075-10166. DOI: <https://doi.org/10.1021/acs.chemrev.6b00057>.
- [5] Z.-Y. Xu, Y. Luo, H. Wang, D.-W. Zhang, Z.-T. Li. Porous Organic Polymers as Heterogeneous Catalysts for Visible Light-Induced Organic Transformations. *Chin. J. Org. Chem.* 2020, 40(11): 3777-3793. DOI: <https://doi.org/10.6023/cjoc202003070>.
- [6] T.-X. Wang, H.-P. Liang, D.A. Anito, X. Ding, B.-H. Han. Emerging Applications of Porous Organic Polymers in Visible-Light Photocatalysis. *J. Mater. Chem. A.* 2020, 8(15): 7003-7034. DOI: <https://doi.org/10.1039/D0TA00364F>.
- [7] T. Zhang, G. Xing, W. Chen, L. Chen. Porous Organic Polymers: A Promising Platform for Efficient Photocatalysis. *Mater. Chem. Front.* 2020, 4(2): 332-353. DOI: <https://doi.org/10.1039/C9QM00633H>.
- [8] C.T.J. Ferguson, K.A.I. Zhang. Classical Polymers as Highly Tunable and Designable Heterogeneous Photocatalysts. *ACS Catal.* 2021, 11(15): 9547-9560. DOI: <https://doi.org/10.1021/acscatal.1c02056>.
- [9] H.-P. Liang, Q. Chen, B.-H. Han. Cationic Polycarbazole Networks as Visible-Light Heterogeneous Photocatalysts for Oxidative Organic Transformations. *ACS Catal.* 2018, 8(6): 5313-5322. DOI: <https://doi.org/10.1021/acscatal.7b04494>.
- [10] J. Luo, J. Lu, J. Zhang. Carbazole-Triazine Based Donor-Acceptor Porous Organic Frameworks for Efficient Visible-Light Photocatalytic Aerobic Oxidation Reactions. *J. Mater. Chem. A.* 2018, 6(31): 15154-15161. DOI: <https://doi.org/10.1039/c8ta05329d>.
- [11] X. Li, X. Ma, F. Zhang, X. Dong, X. Lang. Selective photocatalytic formation of sulfoxides by aerobic oxidation of sulfides over conjugated microporous polymers with thiazolo[5,4-d] thiazole linkage. *Appl. Catal. B: Environ.* 2021, 298: 120514-120623. DOI: <https://doi.org/10.1016/j.apcatb.2021.120514>.
- [12] H. Hao, F. Zhang, X. Dong, X. Lang. 2D sp<sup>2</sup> carbon-conjugated triazine covalent organic framework photocatalysis for blue light-induced selective oxidation of sulfides with O<sub>2</sub>. *Appl. Catal. B: Environ.* 2021, 299: 120691-120702. DOI: <https://doi.org/10.1016/j.apcatb.2021.120691>.
- [13] Z.J. Wang, S. Ghasimi, K. Landfester, K.A.I. Zhang. Molecular Structural Design of Conjugated Microporous Poly(Benzooxadiazole) Networks for Enhanced Photocatalytic Activity with Visible Light. *Adv. Mater.* 2015, 27(40): 6265-6270. DOI: <https://doi.org/10.1002/adma.201502735>.
- [14] V.R. Battula, H. Singh, S. Kumar, I. Bala, S.K. Pal, K. Kailasam, K. Natural Sunlight Driven Oxidative Homocoupling of Amines by a Truxene-Based Conjugated Microporous Polymer. *ACS Catal.* 2018, 8(8): 6751-6759. DOI: <https://doi.org/10.1021/acscatal.8b00623>.
- [15] H. Xu, X. Li, H. Hao, X. Dong, W. Sheng, X. Lang. Designing fluorene-based conjugated microporous polymers for blue light-driven photocatalytic selective oxidation of amines with oxygen. *Appl. Catal. B: Environ.* 2021, 285: 119796-119806. DOI: <https://doi.org/10.1016/j.apcatb.2020.119796>.
- [16] P. Wei, M. Qi, Z. Wang, S. Ding, W. Yu, Q. Liu, L. Wang, H. Wang, W. An, W. Wang. Benzoxazole-Linked Ultrastable Covalent Organic Frameworks for Photocatalysis. *J. Am. Chem. Soc.* 2018, 140(13): 4623-4631. DOI: <https://doi.org/10.1021/jacs.8b00571>.
- [17] Z.-Y. Xu, Y. Luo, D.-W. Zhang, H. Wang, X.-W. Sun, Z.-T. Li. Iridium complex-linked porous organic polymers for recyclable, broad-scope photocatalysis of organic transformations. *Green Chem.* 2020, 22(1): 136-143. DOI: <https://doi.org/10.1039/c9gc03688a>.

- [18] Y. Nailwal, A.D.D. Wonanke, M.A. Addicoat, S.K. Pal. A Dual-Function Highly Crystalline Covalent Organic Framework for HCl Sensing and Visible-Light Heterogeneous Photocatalysis. *Macromolecules*. 2021, 54(13): 6595-6604. DOI: <https://doi.org/10.1021/acs.macromol.1c00574>.
- [19] C. Song, J. Nie, C. Ma, C. Lu, F. Wang, G. Yang. 1,2,3-Triazole-based conjugated porous polymers for visible light induced oxidative organic transformations. *Appl. Catal. B: Environ.* 2021, 287: 119984-119996. DOI: <https://doi.org/10.1016/j.apcatb.2021.119984>.
- [20] Y. Zhi, S. Ma, H. Xia, Y. Zhang, Z. Shi, Y. Mu, X. Liu. Construction of donor-acceptor type conjugated microporous polymers: A fascinating strategy for the development of efficient heterogeneous photocatalysts in organic synthesis. *Appl. Catal. B: Environ.* 2019, 244: 36-44. DOI: <https://doi.org/10.1016/j.apcatb.2018.11.032>.
- [21] W. Zhang, S. Li, X. Tang, J. Tang, C. Pan, G. Yu. Phenothiazine core promoted charge transfer in conjugated microporous polymers for photocatalytic Ugi-type reaction and aerobic selenation of indoles. *Appl. Catal. B: Environ.* 2020, 272: 118982-118992. DOI: <https://doi.org/10.1016/j.apcatb.2020.118982>.
- [22] S. Purser, P.R. Moore, S. Swallow, V. Gouverneur. Fluorine in Medicinal Chemistry. *Chem. Soc. Rev.* 2008, 37(2): 320-330. DOI: <https://doi.org/10.1039/b610213c>.
- [23] R. Berger, G. Resnati, P. Metrangolo, E. Weber, J. Hulliger. Organic Fluorine Compounds: A Great Opportunity for Enhanced Materials Properties. *Chem. Soc. Rev.* 2011, 40(7): 3496-3508. DOI: <https://doi.org/10.1039/c0cs00221f>.
- [24] A.L. Ong, A.H. Kamaruddin, S. Bhatia. Current Technologies for the Production of (S)-Ketoprofen: Process Perspective, *Process Biochem.* 2005, 40(11): 3526-3535. DOI: <https://doi.org/10.1016/j.procbio.2005.03.054>.
- [25] J. Miao, H. Ge. Palladium-catalyzed chemoselective decarboxylative ortho acylation of benzoic acids with  $\alpha$ -oxocarboxylic acids, *Org. Lett.* 2013, 15(12): 2930-2933. DOI: <https://doi.org/10.1021/ol400919u>.
- [26] S.R. Khan, R.T. Berendt, C.D. Ellison, A.B. Ciavarella, E. Asafu-Adjaye, M.A. Khan, P.J. Faustino. Profiles of Drug Substances, Excipients and Related Methodology. 2016, 41: 79-438.
- [27] J.T. Brewster, S. Dell'Acqua, D.Q. Thach, J.L. Sessler. Classics in Chemical Neuroscience: Donepezil, *ACS Chem. Neurosci.* 2019, 10(1): 155-167. DOI: <https://doi.org/10.1021/acschemneuro.8b00517>.
- [28] A. Sagadevan, V.P. Charpe, A. Ragupathi, K.C. Hwang. Visible Light Copper Photoredox-Catalyzed Aerobic Oxidative Coupling of Phenols and Terminal Alkynes: Regioselective Synthesis of Functionalized Ketones via  $C\equiv C$  Triple Bond Cleavage. *J. Am. Chem. Soc.* 2017, 139(8): 2896-2899. DOI: <https://doi.org/10.1021/jacs.6b13113>.
- [29] S. Bloom, C.R. Pitts, D.C. Miller, N. Haselton, M.G. Holl, E. Urheim, T. Lectka. A Polycomponent Metal-Catalyzed Aliphatic, Allylic, and Benzylic Fluorination. *Angew. Chem. Int. Ed.* 2012, 51: 10580-10583. DOI: <https://doi.org/10.1002/ange.201203642>.
- [30] J.-B. Xia, C. Zhu, C. Chen. Visible Light-Promoted Metal-Free C-H Activation: Diarylketone-Catalyzed Selective Benzylic Mono- and Difluorination. *J. Am. Chem. Soc.* 2013, 135(46): 17494-17500. DOI: <https://doi.org/10.1021/ja410815u>.
- [31] B. Pieber, M. Shalom, M. Antonietti, P.H. Seeberger, K. Gilmore. Continuous Heterogeneous Photocatalysis in Serial Micro-Batch Reactors, *Angew. Chem. Int. Ed.* 2018, 57(31): 9976-9979. DOI: <https://doi.org/10.1002/ange.201712568>.
- [32] P. Mondal, M. Lovisari, B. Twamley, A.R. McDonald. Fast Hydrocarbon Oxidation by a High Valent Nickel-Fluoride Complex. *Angew. Chem. Int. Ed.* 2020, 59(31): 13044-13050. DOI: <https://doi.org/10.1002/anie.202004639>.
- [33] J.K. Bower, A.D. Cypcar, B. Henriquez, S.C.E. Stieber, S. Zhang.  $C(sp^3)$ -H Fluorination with a Copper(II)/(III) Redox Couple. *J. Am. Chem. Soc.* 2020, 142: 8514-8521. DOI: <https://doi.org/10.1021/jacs.0c02583>.
- [34] M.B. Andrus. Allylic and benzylic oxidation. In *Science of Synthesis, Stereoselective Synthesis*, 1st ed.; J.G.D. Vries, G.A. Molander, P.A. Evans, Eds.; Thieme Verlag: Stuttgart., 2011, 469-482.
- [35] F. Goubard, F. Dumur. Truxene: A Promising Scaffold for Future Materials. *RSC Adv.* 2015, 5: 3521-3551. DOI: <https://doi.org/10.1039/c4ra11559g>.
- [36] K. Shi, J.-Y. Wang, J. Pei.  $\pi$ -Conjugated Aromatics Based on Truxene: Synthesis, Self-Assembly, and Applications. *Chem. Rec.* 2015, 15(1): 52-72. DOI: <https://doi.org/10.1002/tcr.201402071>.
- [37] S. Das, H. Kim, K. Kim. Metathesis in Single Crystal: Complete and Reversible Exchange of Metal Ions Constituting the Frameworks of Metal-Organic Frameworks. *J. Am. Chem. Soc.* 2009, 131(11): 3814-3815. DOI: <https://doi.org/10.1021/ja808995d>.
- [38] L. Liu, S.G. Telfer. Systematic Ligand Modulation Enhances the Moisture Stability and Gas Sorption Characteristics of Quaternary Metal-Organic Frameworks. *J. Am. Chem. Soc.* 2015, 137(11): 3901-3909. DOI: <https://doi.org/10.1021/jacs.5b00365>.
- [39] Q. Zhang, C. Zhang, L. Cao, Z. Wang; B. An, Z. Lin, R. Huang; Z. Zhang, C. Wang, W. Lin., Förster Energy Transport in Metal-Organic Frameworks Is Beyond Step-by-Step Hopping. *J. Am. Chem. Soc.* 2016, 138(16): 5308-5315. DOI: <https://doi.org/10.1021/jacs.6b01345>.
- [40] X. Yang, Y. Hu, N. Dunlap, X. Wang, S. Huang, Z. Su, S. Sharma Y. Jin, F. Huang, X. Wang, S.-H. Lee, W. Zhang. A Truxenone-based Covalent Organic Framework as an All-Solid-State Lithium-Ion Battery Cathode with High Capacity. *Angew. Chem. Int. Ed.* 2020, 59: 20385-20389. DOI: <https://doi.org/10.1002/anie.202008619>.

- [41] K. Lin, Z. Wang, Z. Hu, P. Luo, X. Yang, X. Zhang, M. Rafiq, F. Huang, Y. Cao. Amino-Functionalised Conjugated Porous Polymers for Improved Photocatalytic Hydrogen Evolution. *J. Mater. Chem. A.* 2019, 7(32): 19087-19093. DOI: <https://doi.org/10.1039/c9ta06219j>.
- [42] H. Zhang, C. Zhou, Y. Zheng, X. Zhang. Isotruxene-Based Porous Polymers as Efficient and Recyclable Photocatalysts for Visible-Light-Induced Metal-Free Oxidative Organic Transformations. *Green Chem.* 2021, 23(22): 8878-8885. DOI: <https://doi.org/10.1039/D1GC03165A>.
- [43] E.V. Dehmlow, T. Kelle. Synthesis of New Truxene Derivatives: Possible Precursors of Fullerene Partial Structures? *Synth. Commun.* 1997, 27(11): 2021-2031. DOI: <https://doi.org/10.1080/00397919708006804>.
- [44] C. Zhou, W. Xuan, S.-P. Luo, Y.-H. Bao. One-step, Large-scale Synthesis of Isotruxene. *J. Chem. Res.* 2018, 42(11): 556-557. DOI: <https://doi.org/10.3184/174751918x15403823022089>.